Nuclear Magnetic Resonance Studies of the 1,4-Cyclohexanedione−Bromate−Acid Oscillatory System

Melanie M. Britton[†]

Magnetic Resonance Research Centre, Department of Chemical Engineering, University of Cambridge, New Museums Site, Pembroke Street, Cambridge, CB2 3RA, U.K.

Received: February 7, 2003

The 1,4-cyclohexanedione-bromate-acid oscillating system was investigated using nuclear magnetic resonance (NMR) techniques. A range of NMR experiments were used which imaged pattern formation during the oscillations, probed the organic chemistry, and observed the presence of convection. Measurements of the change in concentration of key organic species, 1,4-cyclohexanedione, 2-bromo-1,4-cyclohexanedione, and 1,4-benzoquinone, with concurrent imaging of patterns, allowed partial validation of proposed reaction mechanisms. An investigation of the presence of convection, arising through density differences produced by the reaction, was made. It was found that convection was present in reaction solutions contained within 10 mm NMR tubes, but not 5 mm tubes. Pulsed gradient spin−echo (PGSE) experiments measuring the displacement of the solvent molecules found the dispersion (mobility) coefficients for the solvent increased, on average, by a factor of 3, from 1.3×10^{-9} m^2 s^{-1} to 3.9×10^{-9} m^2 s^{-1} ($\pm 0.02 \times 10^{-9}$ m^2 s^{-1}), in the vertical direction where convection was present.

Introduction

For many years the Belousov−Zhabotinsky (BZ)[1,2] reaction has been the pre-eminent reaction used in the study of oscillations and pattern formation in chemical systems. This reaction is based on the catalyzed oxidation of malonic acid by bromate, and the concentrations of certain intermediates, such as bromide ions and bromous acid, are found to oscillate. The catalyst used is a transition metal such as cerium, iron, or manganese, and concentrations of the oxidized and reduced states of these ions also oscillate. It is the oscillations of the catalyst which produce color changes of the solution during the reaction. In the case of the ferroin-catalyzed reaction, where the reaction is stirred, color oscillations between red and blue are observed. Where the solution is left unstirred, waves and patterns form.

Current techniques used to study pattern formation in the BZ, and similar reactions, rely on the color changes produced by the catalyst, and patterns are recorded using photographic methods. Magnetic resonance imaging (MRI) applied to the BZ reaction, by the group of Armstrong,[3−5] has been shown to be successful. While conventional visualization of pattern formation is through the color changes of indicators, MRI relies on relaxation time differences between water surrounding the oxidized metal ions, which are associated with the waves, and water surrounding the reduced metal ions, which are located predominantly outside the waves. Previous MRI studies of the BZ reaction have focused on the improvement of image contrast[5] and, by using MRI as a purely imaging technique, have studied kinematic wave dynamics[6] and the effect of convection instabilities on waves.[7] While MRI has some advantages over more conventional imaging methods, the potential for NMR to unravel many of the complexities of these systems can go much further than imaging pattern formation. Work by Schlüter and Weiss[8] and Hansen and Ruoff[9] showed how the relaxation time, line width, and chemical shift of water oscillated during the BZ reaction in batch conditions. Also NMR studies of the methylmalonic acid BZ reaction were made by Hansen and coworkers, who investigated the main organic products and intermediates, formed in this reaction. This paper explores the application of a wider range and combination of NMR techniques to studying oscillations and pattern formation in a chemical system.

A valuable alternative to the classic BZ reaction is the 1,4-cyclohexanedione (CHD)-bromate-acid[10,11] uncatalyzed bromate oscillator (UBO). While they share some similar chemistry and both display rich oscillatory and pattern-forming behavior,[2,12,13] the CHD system has some key differences. Unlike the BZ reaction, this system does not produce carbon dioxide bubbles. The reason for this is based on the different chemistry of the organic species in these systems. In the BZ reaction oxidation of the bromomalonic acid results in its cleavage and production of CO_2 gas.[14] Production of CO_2 gas leads to the formation of bubbles, which disrupt the patterns and can also affect nuclear magnetic resonance (NMR) experiments. In the CHD system the oxidation of the brominated organic species does not result in the cleavage of the aliphatic rings, but rather in an aromatization;[14] thus the production of CO_2 is prevented. Another advantage with this system is that it displays long-lasting oscillations. This is due to one of the main reducing agents, 1,4-dihydroxybenzene (hydroquinone), being generated slowly, and continuously, during the reaction and only small portions ($<10^{-5}$ M) of reactants being consumed during a single oscillatory phase. However even though this system has clear advantages, there remain some uncertainties concerning its chemistry, and this has limited its more widespread use. To date no spectroscopic studies have been performed in conjunction with MRI imaging experiments, and no NMR spectroscopic measurements of the organic chemistry of the CHD oscillator have been made. This paper presents the first MRI images of pattern formation in the CHD uncatalyzed bromate oscillator.

[†] E-mail: melanie_britton@cheng.cam.ac.uk.

10.1021/jp0343279 CCC: $25.00
Published on Web 05/20/2003

TABLE 1: Reaction Steps Involving Organic Molecules from the Reaction Mechanism of Szalai and Körös[14]

R1	$CHD + H^+ \rightleftharpoons CHDE + H^+$
R2	$CHDE + Br_2 \rightarrow BrCHD + H^+ Br^-$
R3	$CHDE + HOBr \rightarrow BrCHD + H_2O$
R4	$BrCHD \rightarrow CHED + H^+ + Br^-$
R5	$CHED + H+ \rightarrow H_2Q + H^+$
R6	$H_2Q + Br_2 \rightarrow Q + 2Br^- + 2H^+$
R7	$H_2Q + H^+ + BrO_3^- \rightarrow Q + HBrO_2 + H_2O$
R8	$H_2Q + HOBr \rightarrow Q + Br^- + H^+ + H_2O$
R9	$CHD + H^+ + BrO_3^- \rightarrow H_2Q + HBrO_2 + H_2O$
R10	$H_2Q + BrO_2^\bullet \rightarrow HQ^\bullet + BrO_2$
R11	$HQ^\bullet + BrO_2^\bullet \rightarrow Q + HBrO_2$
R12	$2\ HQ^\bullet \rightleftharpoons H_2Q + Q$

[a] Abbreviations used for the organic molecules are CHD = 1,4-cyclohexanedione, CHDE = enol form of CHD, BrCHD = 2-bromo-1,4-cyclohexanedione, H_2Q = 1,4-hydroquinone, and Q = 1,4-benzoquinone.

NMR spectra, taken during oscillations, are also presented for the first time for the CHD reaction. For imaging purposes, a manganese indicator is used in order to visualize the waves, even though this is an uncatalyzed oscillator. Manganese is found[5] to be more stable than ferroin and produces, in dilute concentrations, good relaxation time contrast between the two oxidative states, Mn^{2+} and Mn^{3+}.

In this reaction the main organic species formed have been identified[13] as the intermediates 2-bromo-1,4-cyclohexanedione, BrCHD, and hydroquinone (1,4-dihydroxybenzene), H_2Q, and the product quinone (1,4-benzoquinone), Q. The formation and reaction of hydroquinone are keys to the oscillatory nature of the system, and this makes this system very interesting to study with NMR. Namely, with organic species involved in key reaction steps, there is an opportunity to study directly the chemistry, which underpins the oscillatory and pattern forming nature of this system. The organic chemistry of this reaction is not fully understood, and direct measurements using NMR can lead to further validation of proposed reaction mechanisms.[14] Such a validation is of significant importance as it is believed that a drawback, with the application of this system to the study of nonlinear chemical behavior, is its less understood organic chemistry,[15] compared to the BZ reaction. This paper will present spectra, for the CHD oscillator during pattern formation, which follow the reaction of 1,4-cyclohexanedione and the major intermediates and products.

A detailed reaction mechanism for this system has been devised[14−16] through analysis of isolated reaction steps and by analysis of the complete reaction from samples removed at regular intervals during oscillations. The steps involving organic molecules, which are of most interest in this study, are shown in Table 1. Direct verification of several key reaction steps, particularly those involving the formation of hydroquinone, have not previously been possible. Oscillations within this system have been monitored by measuring the redox potential of the solution using a platinum and reference electrode. These oscillations have been assumed to originate from the hydroquinone and quinone redox pair, and the periodic change in redox potential is believed to mimic the oscillating changes in concentration of H_2Q. Simulations of this system can mimic this behavior successfully and have found that the relative concentration of hydroquinone does oscillate in a similar way to the redox oscillations.[14] However, previous studies were not able to directly measure the changes in concentration of any of the organic molecules. By application of NMR, a unique and valuable window into the chemistry of the system is possible along with independent verification of the reaction mechanism.

In addition to the study of the chemistry of this system, the hydrodynamics have also be probed directly using NMR methods. Convection can play a major role in the BZ and CHD reactions, as there are density differences between solution inside and outside the waves, arising, predominantly, from the differences in the chemical composition.[17] Convection is frequently considered a problem in the study of traveling waves and pattern formation, so steps are often taken to remove it. In aqueous solution the fluid is often confined to a narrow tube or a thin layer in a Petri dish. Another method is to increase the viscosity of the solution by the addition of a polymer. However this introduces an extra level of complexity to the system, as interactions between the reacting molecules and the solvent medium cannot be ruled out.[18] Apart from its often-considered inconvenience, the presence of convection is of interest, in its own right, in such chemical systems. Reaction−diffusion mechanisms account for a range of wave- and pattern-forming behavior in the BZ and similar reactions; however they do not take convection into account. The study of combined reaction−diffusion and convection models is a rich area of research, not least for its applicability to biological systems, where convection is not so conveniently removed. A clear understanding of the onset and development of convection is required for such models.

Convection has been observed previously in the CHD system[17] by studying the effect on wave structure and velocity, a commonly used method for probing convection.[19,20] Papers by Miike and co-workers[21,22] presented experiments using a 2-D microscope video-imaging technique, to study convection in chemical waves in the BZ reaction, where the velocity of dispersed particles was measured. While they were able to image the waves and measure velocities at a local level, they were unable to measure the velocity of the solution simultaneously as a whole. Also this technique is more suited to the observation of surface motion, in a thin layer, and not three-dimensional volumes. The NMR techniques presented in this paper do not rely on the interpretation of effects on the wave or use tracer particles, but directly probe the motion of the molecules. This is the first application of MRI measurements of mass transport in these systems and has several advantages over methods previously used to study convection. Direct measurement of hydrodynamic motion is possible and, with the use of fast imaging, the opportunity to visualize directly convective motion becomes possible. Bulk diffusion coefficients and local convective velocities were measured.

Experimental Section

Materials. The reaction was carried out in batch conditions, and the reactant concentrations were chosen to produce the maximum number of oscillations possible.[13] In the reactions presented in this paper, $MnSO_4$ was used instead of ferroin, at a concentration that was considered to be below that which affects the rate of reaction or promotes additional reaction steps.[15] The reacting solution was 2.5 M H_2SO_4 (Aldrich), 0.1 M 1,4-cyclohexanedione (Aldrich), 0.1 M $NaBrO_3$ (Fluka), and 2.5×10^{-4} M $MnSO_4$ (BDH). All reactants were used with no further purification. This concentration of $MnSO_4$ was identified to give the best relaxation time contrast[23] of the water molecules, between oxidative and reductive states of the metal ion, allowing the waves to be clearly resolved.

NMR Methods. The NMR spectrometer used was a Bruker DMX-300, which comprises a 7.0-T superconducting magnet, operating at a proton resonance frequency of 300 MHz, and equipped with shielded gradient coils, which provide a maximum gradient strength of 1 T m^{-1}. All NMR experiments were

done at a temperature of 20 ± 0.2 °C. Experiments using a 5 mm NMR tube were put into a 15 mm radio frequency (rf) resonator, which had a 90° pulse of ≈12 μs, and experiments using a 10 mm NMR tube were performed in a 25 mm rf coil, which had a 90° pulse length of ≈30−60 μs. The ionic strengths of the reaction solutions were sufficiently high that it was not possible to tune the coils with greater filling factors. Pulse lengths were sensitive to the ionic strength of the reaction mixture. All NMR data were analyzed with the software package PROSPA.[24] PROSPA was used to analyze the reconstructed images produced by the spectrometer software. Analysis of the NMR spectra, by fitting the data using a multicomponent Lorentzian fit, provided peak amplitudes and integrals.

Experiments[25] were performed to measure the spin−lattice, T_1, and spin−spin, T_2, relaxation times of solutions containing oxidized or reduced states metal ions at a range of concentrations. T_2 relaxation measurements were obtained using a CPMG sequence using a tau of 0.5 ms and collecting up to 250 echoes. T_1 measurements used a saturation recovery experiment consisting of a presaturation train of 90° rf pulses and crusher gradients, with a recovery delay before signal acquisition. A series of 25 experiments were collected, varying the recovery delay exponentially from 5 μs to 12 s. At the Mn concentration, 2.5×10^{-4} M, the T_2 relaxation times for water surrounding the reduced (Mn^{2+}) and oxidized (Mn^{3+}) states were 17.0 ± 0.1 ms and 66.0 ± 0.1 ms, respectively. The T_1 relaxation times were 354 ± 5 ms (Mn^{2+}) and 660 ± 6 ms (Mn^{3+}). From these measurements the parameters used for imaging were selected to produce the best image quality.

Images were produced using the fast imaging technique RARE.[26] This robust imaging technique is based on a single excitation, multiple spin−echo sequence. An advantage with this sequence is that images are dependent on T_2, not T_2*,[23] and if the relaxation time of the system is longer than the echo train duration, an image can be obtained in one shot. This makes experiments very rapid, and typical times for experiments of between 1 and 4 s were possible. Images were produced in both 5 mm and 10 mm NMR tubes. The 5 mm tube images comprised a 256 (vertical) × 64 (horizontal) pixel array with fields of view of 60 mm and 10 mm, respectively and a slice thickness of 1 mm, through the center of the tube. The 10 mm tube images comprised a 256 (vertical) × 64 (horizontal) pixel array with fields of view of 60 mm and 15 mm, respectively, also with a slice thickness of 1 mm. The relatively short T_2 relaxation times of the systems required a RARE factor of 16, which meant four acquisitions were needed, which were separated by a repetition time of 1 s. Images were cropped to remove regions of no signal, leaving the observable regions of the coils, which were 36 mm, in the vertical direction, for the 15 mm rf coil and 4.1 mm for the 25 mm rf coil.

Measurements of bulk molecular displacement were obtained using a pulse gradient spin−echo (PGSE) method.[23] Here diffusion coefficients were obtained through the analysis of the signal attenuation produced by two magnetic field gradient (**q**) pulses.[27] Typical values for PGSE parameters included a $\mathbf{g}_{max}$ of 40 G/cm, with 64 gradient steps going from $+\mathbf{g}_{max}$ to $-\mathbf{g}_{max}$, an observation time, Δ, of 100 ms, and gradient duration, δ, of 3 ms. The number of signal averages was 2, with a repetition time of 1 s, and experiments typically took 60−70 s. In the systems where diffusion coefficients were enhanced and convection was believed to be present, the velocity of the fluid was further probed using a series of RARE MRI images where a DANTE[28] preconditioning sequence had been applied. The DANTE sequence superimposes a grid of magnetization, in this case in two dimensions, which is distorted, through coherent motion during a waiting time between the DANTE sequence and image acquisition. The grid spacing was 2 mm, and the waiting time ranged from 6.4 to 400 ms. The upper limit on the waiting time is determined by blurring of the grids, due to T_1 relaxation and molecular diffusion. Each experiment took on the order of 5 s.

For the spectroscopy experiments water signal suppression sequences were necessary as the molecules of interest were in dilute (<0.1 M) aqueous solution. For solvent suppression, two pulse sequences were used: WATERGATE[29] and P1$\bar{3}3\bar{1}$.[30] WATERGATE is a spin−echo technique using two gradient pulses, one on each side of the 180° rf pulse, which respectively dephase and refocus the magnetization. The solvent suppression characteristics are derived from the nature of the 180° pulse, which is frequency selective, with a null in the frequency spectrum. If this null is positioned at the resonant frequency of the solvent (water) peak, then these spins will not experience the 180° flip pulse, and so the second gradient pulse will further dephase, rather than refocus, thus suppressing this peak. The sequence P1$\bar{3}3\bar{1}$ is based on a simple "jump and return" sequence. Here two 90° pulses of opposite phase are separated by a dephasing time, τ. The carrier frequency is positioned on the peak to be suppressed, so after the first 90° pulse spins at different frequencies will dephase, within the rotating frame, while this solvent peak remains "on-resonance". The spins that dephase during the period τ will retain a component in the transverse plane after the second rf pulse and hence will produce a signal during acquisition. The solvent peak, however, is fully rotated to the longitudinal axis by the second 90° rf and so the signal from these spins is suppressed. This jump and return sequence is written as $1\bar{1}$, where the overbar indicates the two 90° rf pulses are out of phase. The sequence P1$\bar{3}3\bar{1}$ is based on this simple experiment; however instead of two 90° pulses, four pulses are used which have pulse lengths in the ratio of 1:3:3:1. This sequence has improved characteristics[31] over the simpler $1\bar{1}$ sequence, but still remains relatively simple. A disadvantage with this sequence is that the null is periodic; therefore peaks with an offset of $1/2\tau$, $1/\tau$, etc. will also be nulled. Also peaks between these nulls will have their amplitude modulated as a function of τ.

In the spectra presented in this paper, the best signal suppression was produced by the P1$\bar{3}3\bar{1}$ sequence; however some baseline correction was necessary and it was not possible to achieve adequate water suppression and observe all the organic species simultaneously. A delay, τ, of 330 μs was used, which produced a second null 5 ppm away from the water peak. This gave the best water suppression with maximum signal for the CHD and neighboring peaks (2.5−3 ppm). However peaks near this water signal were also suppressed. To observe peaks, such as quinone, near the water signal, a delay of 900 μs was necessary; this produced a second null at 1.85 ppm about the water peak, which however suppressed the CHD and neighboring peaks. To observe both the regions of the spectrum containing both quinone (Q) and CHD, WATERGATE was found to be better. A delay between the composite 180 pulses of 660 μs was used. The gradient strength and duration in the WATERGATE experiments were 5 G/cm and 500 μs, respectively. As both sequences have advantages, they have both been used in the study of this reaction.

Kinetic Simulations. For comparison with experimental data, the reaction mechanism, proposed by Szalai and Körös,[14] was simulated by the program *Chemical Kinetics Simulator*.[32] In these simulations 5.0×10^8 particles were used and the reaction

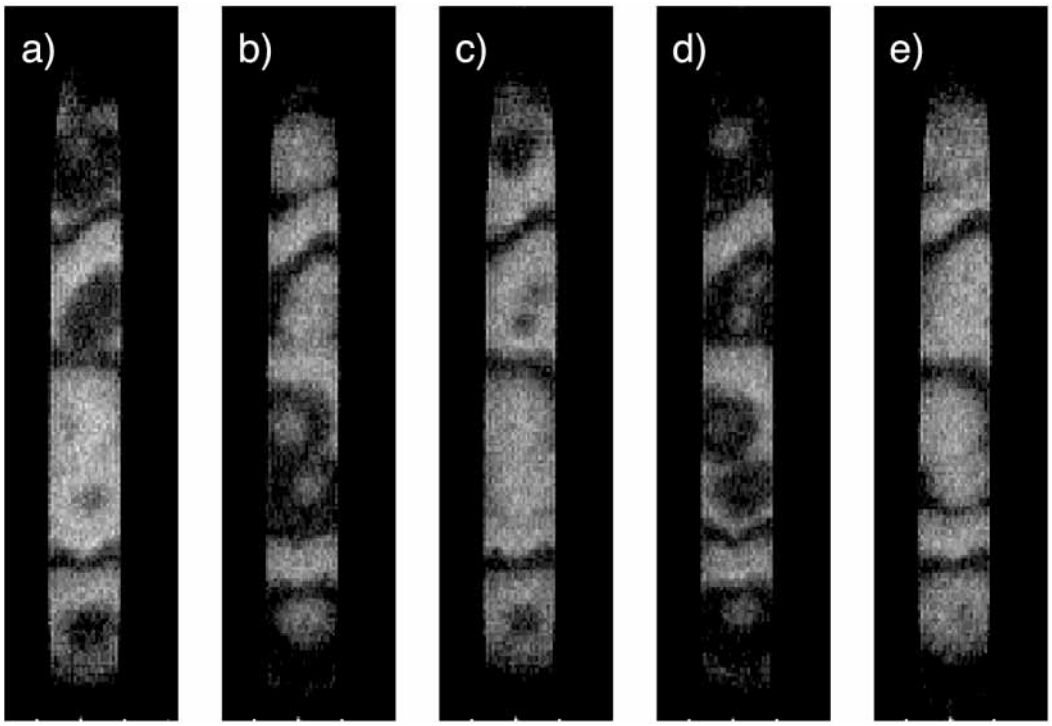

Figure 1. MRI images of initial pattern formation in the 1,4-cyclohexanedione oscillator in a 5 mm tube. Image (a) was taken 2100 s after the reagents were mixed, with subsequent images acquired at an interval of 18 s. Each image is a 256 × 64 pixel array with a vertical field of view of 60 mm and a horizontal field of view of 10 mm. The images have a slice thickness of 1 mm and are taken from the center of the tube. Images have been cropped to remove regions of no signal and leave only the observable region of the rf coils.

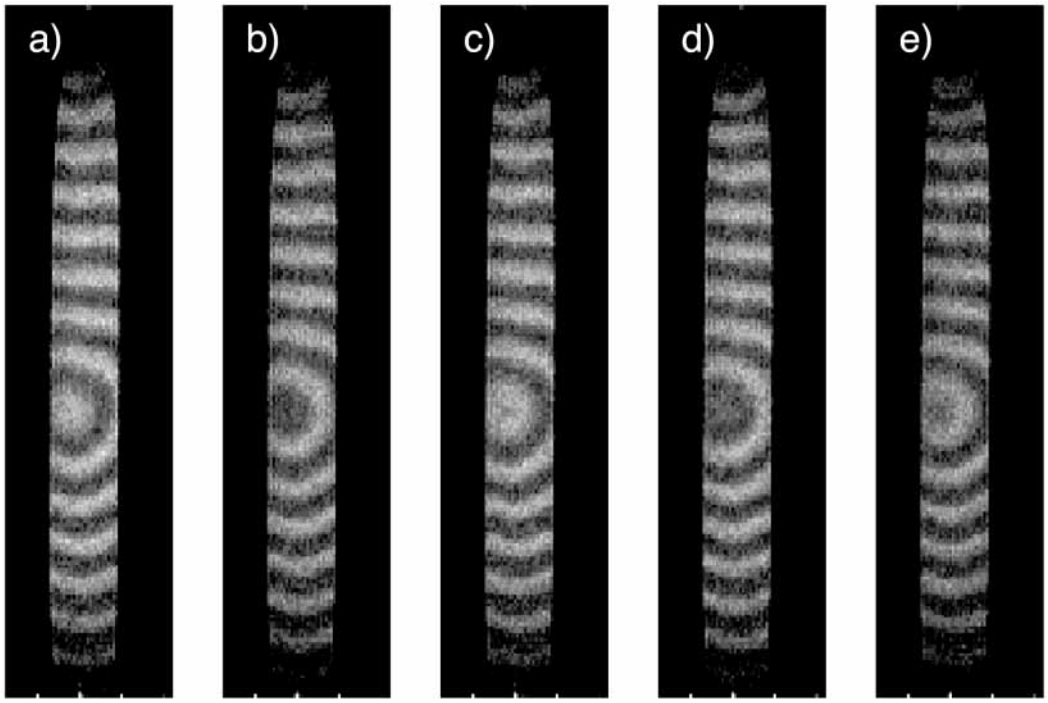

Figure 2. MRI images of trigger wave formation in the 1,4-cyclohexanedione oscillator, in a 5 mm tube, obtained toward the end of oscillations. Image (a) was taken 3280 s after the reagents were mixed, with subsequent images (b−e) acquired at an interval of 18 s. Imaging parameters are the same as Figure 1. The width of the waves was measured at 2.3 ± 0.2 mm.

conditions were 1 atm and 20 °C. The starting concentrations used in the simulations were identical to the concentrations used experimentally.

Results

A series of images were taken for the reaction during pattern formation. Figure 1 shows patterns formed in 5 mm tubes; these images were acquired at the start of pattern formation. Typically these early patterns show several excitation centers, from which waves propagate outward and interact with other waves and the walls of the vessel. After several minutes the number of excitation points decreases and one or two main ones remain. Trigger waves[12] are frequently observed toward the end of the reaction oscillatory period; typical images are shown in Figure

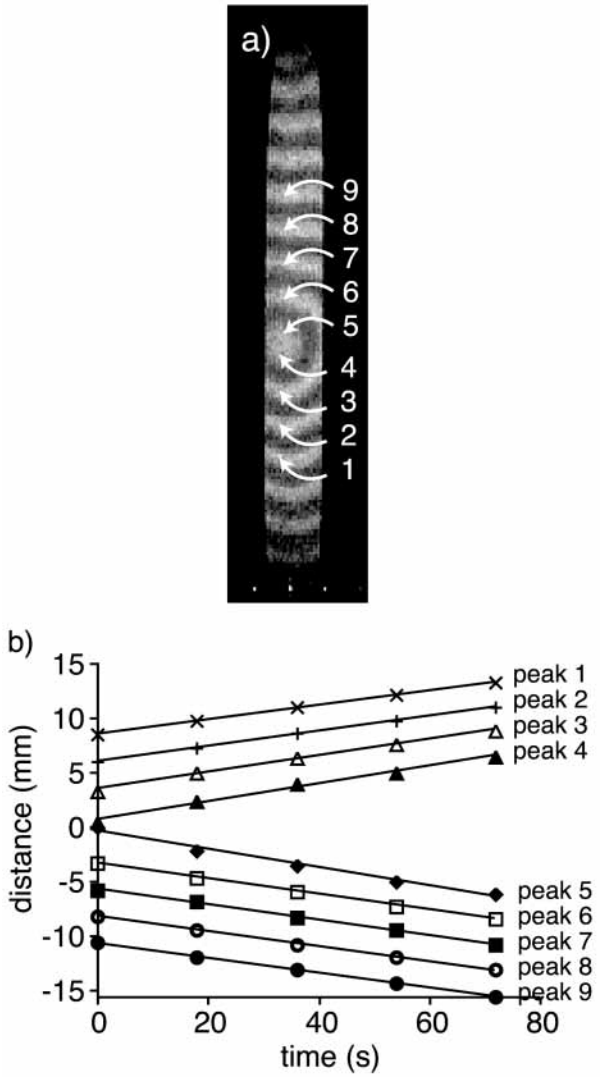

Figure 3. (a) Image of trigger waves taken at 3280 s (Figure 2a) after mixing, indicating the peak numbering used in the peak position vs time plot (b) and peak velocity table (Table 2). (b) Plot of distance from excitation site vs time, following the displacement of the peaks shown in the images in Figure 2a−e.

2. The excitation point is in the center of the image, and the waves are seen to propagate upward and downward in the tube. Chemical wave velocities can be measured from the series of images in Figure 2. The position of the wave was measured from signal intensity profiles taken down the horizontal center of the wave. The wave position, vertically, was then measured from the center of the wave, corresponding to the region of high signal intensity, to within an accuracy of ±1 pixel (pixel diameter is 234 μm). A plot displaying wave position against time for selected waves is shown in Figure 3, and the calculated velocities are given in Table 2. It can be seen that each wave moves at a constant velocity and that the simultaneously created upward and downward waves move at similar velocities. However each subsequently formed wave moves at a velocity higher than the previously formed wave. This has also been observed by Steinbock et al.[33]

TABLE 2: Wave Velocities for the Waves Identified in Figure 3

peak no.	wave velocity/ mm s^{-1} ($\pm$0.003 mm s^{-1})	peak no.	wave velocity/ mm s^{-1} ($\pm$0.003 mm s^{-1})
1	0.067	6	0.071
2	0.069	7	0.07
3	0.076	8	0.068
4	0.082	9	0.069
5	0.084		

Other patterns have been observed in this reaction. Figure 4 shows a set of images, which were taken toward the end of pattern formation, where a crossing wave pattern is observed. This pattern is set up toward the top of the image and moves down through the solution, as shown in subsequent images. The formation of these patterns is most likely through the presence of two excitation centers, near the walls of the tube, which simultaneously produce waves that move through the reaction medium and interfere with each other as they meet in the center of the tube.

The presence of convection was investigated, as it was considered possible that the 5 mm NMR tube was potentially wide enough for convection to occur.[17] However as the images of the CHD reaction in the 5 mm tubes were undistorted and the velocity of waves moving upward and downward were comparable, there was a strong indication of the absence of convective motion. This was further corroborated by a diffusion measurement of the fluid using PGSE measurements. It was found that the diffusion coefficient, at 20 °C, for water was $(1.3 \pm 0.002) \times 10^{-9}$ m^2 s^{-1}, which is consistent with the diffusion coefficient expected for water, in fast exchange with sulfuric acid. Diffusion coefficients, also at 20 °C, for the

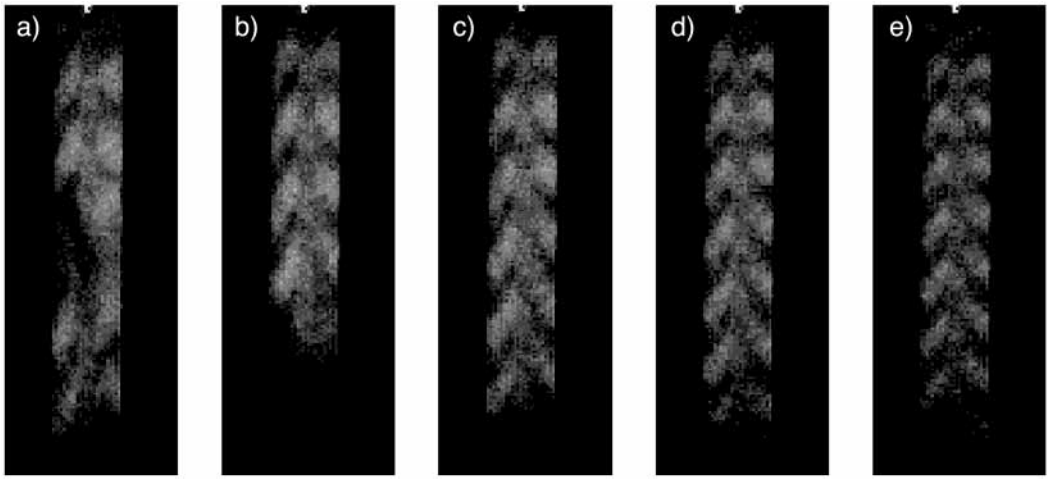

Figure 4. MRI images of crossing waves, in a 5 mm tube, obtained toward the end of oscillations. The interval between images (a−e) was 20 s. Imaging parameters are the same as Figure 1.

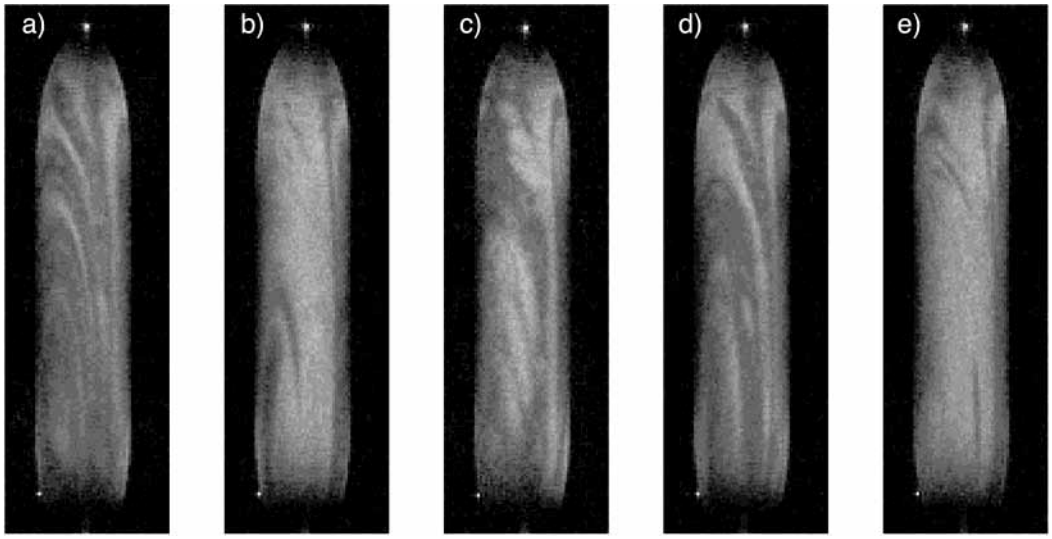

Figure 5. MRI images of pattern formation in the 1,4-cyclohexanedione oscillator, in a 10 mm NMR tube, where convection is present. Image (a) was taken 2220 s after the reagents were mixed, with subsequent images acquired at an interval of 22 s. Each image is a 256 × 64 pixel array with a field vertical of view of 60 mm and a horizontal field of view of 15 mm. Images have a slice thickness of 1 mm and are taken from the center of the tube.

organic molecules 1,4-cyclohexanedione, 2-bromo-1,4-cyclohexanedione (BrCHD), and quinone (Q) were measured at $(1.2 \pm 0.02) \times 10^{-9}$ m^2 s^{-1}, $(1.2 \pm 0.02) \times 10^{-9}$ m^2 s^{-1}, $(1.26 \pm 0.02) \times 10^{-9}$ m^2 s^{-1}, respectively. It should be noted that as this reaction is very slow on the time scale of the NMR experiment, the effect of changing concentrations during reaction is negligible.

Diffusion measurements taken for water molecules, taken 27 min after mixing and 7 min after patterns appeared in a 10 mm tube, give a transport coefficient, measured in the vertical direction, of $(3.9 \pm 0.2) \times 10^{-9}$ m^2 s^{-1}, which is three times larger than normal. As this is an indication of the presence of convection, these transport coefficients should be considered as dispersion, rather than diffusion, coefficients. The dispersion coefficients for CHD and BrCHD were similarly elevated at a value of $(3.8 \pm 0.3) \times 10^{-9}$ m^2 s^{-1}. This indicator of convection is borne out in the images, shown in Figure 5. Here a series of images were obtained at intervals of 22 s. The heterogeneity of the signal intensity is produced by chemical waves; however they propagate in a random manner and are dependent on underlying fluid motion. Diffusion measurements during the reaction show that convection is present and starts before the formation of waves and persists throughout the reaction. Molecular transport measurements taken in the horizontal direction give a diffusion coefficient of $(1.3 \pm 0.003) \times 10^{-9}$ m^2 s^{-1}, which indicates convection operates predominantly in the vertical plane and is consistent with convective flow produced through density changes. Measurements taken subsequently found that the dispersion coefficients became smaller as the reaction progressed.

To get a more complete picture of the convective flow field, an NMR image visualizing the flow was taken. A set of images were acquired during the reaction undergoing convective motion, which had been preconditioned with a DANTE magnetization grid. The image in Figure 6a had a delay of 6.4 ms between DANTE preconditioning and image acquisition. During this time the motion of fluid was negligible, and so the grid remains essentially undistorted. The image shown in Figure 6b had a delay of 400 ms, and during this time there was significant motion, which resulted in an observable distortion of the grid. By use of the two images and measurement of the grid displacement between the two images, over the time difference,

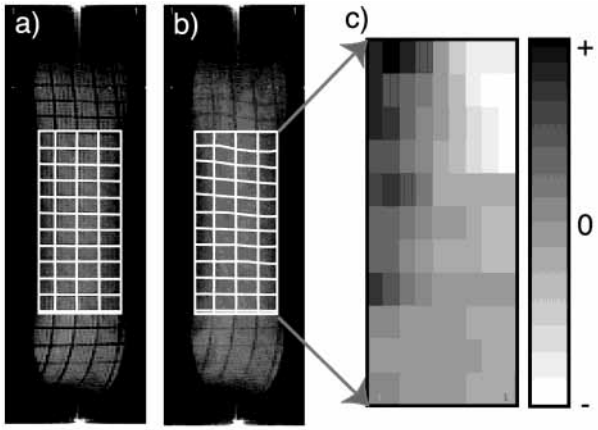

Figure 6. (a) DANTE tagged MRI image, where a waiting time of 6.4 ms was used between tagging and image acquisition. (b) DANTE tagged MRI image, where a waiting time of 400 ms was used. The centrally tagged region has been highlighted where the magnetic field gradient is linear, and from this region the velocity map, shown in (c), is derived. (c) Velocity map of convection calculated from images (a) and (b). The black and white scale represents velocities from −0.9 mm s^{-1} (black) to +0.9 mm s^{-1} (white).

the velocity of the fluid was calculated. Figure 6c shows a velocity map for the fluid in the central section of the tube during oscillations and was taken 38 min after the reactants were mixed. The image shows positive and negative velocities in the vertical direction, up to a maximum of ±0.9 mm s^{-1}. As can be seen from image 5b, the grid is only distorted vertically and not horizontally. This shows that for this 1 mm central slice there is little transport normal to the direction of gravity and is in agreement with the PGSE diffusion measurements. It was observed that the convection was not stable in this geometry, and so only rapid velocity imaging techniques were possible. While this velocity image clearly shows the presence of convection, it does not show the full structure of this convective flow. The image shows regions of highest flow velocities at the top corners, which are in opposite directions. It is unlikely that this represents a single circulatory flow pattern, which is in the plane of the image, as there is no corresponding horizontal motion underneath. It is possible that this image shows a portion of two, or more, circulating flow fields which are counter-

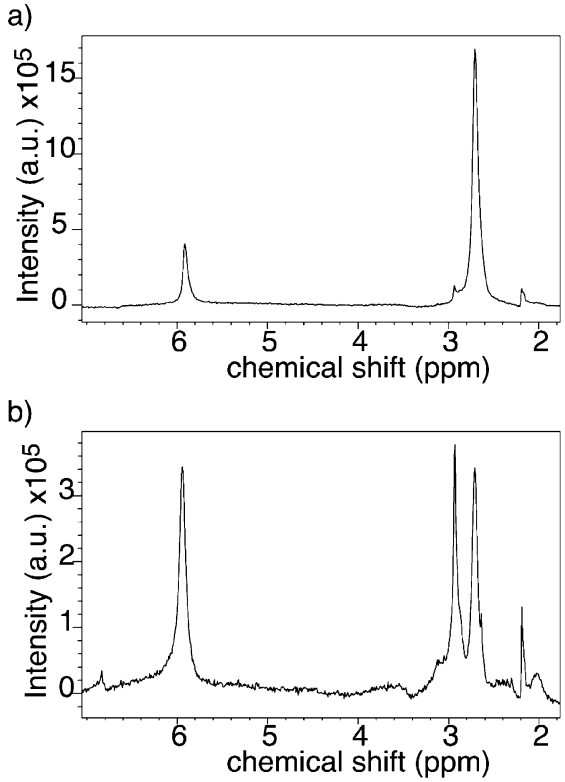

Figure 7. Spectra using the P1$\bar{3}3\bar{1}$ sequence. Spectrum (a) was obtained 540 s after the reagents were first mixed and spectrum (b) at 4155 s. Spectra were acquired with eight signal averages, a repetition time of 10 s, and a τ of 330 μs. Peaks at 2.7 ppm, 2.92 ppm, 5.94 ppm, and 6.83 ppm have been identified as CHD, BrCHD, H_2O/H_2SO_4, and Q, respectively. Minor peaks at 3.04, 2.62, 2.17, and 2.0 ppm are also observed; further work is required to assign these.

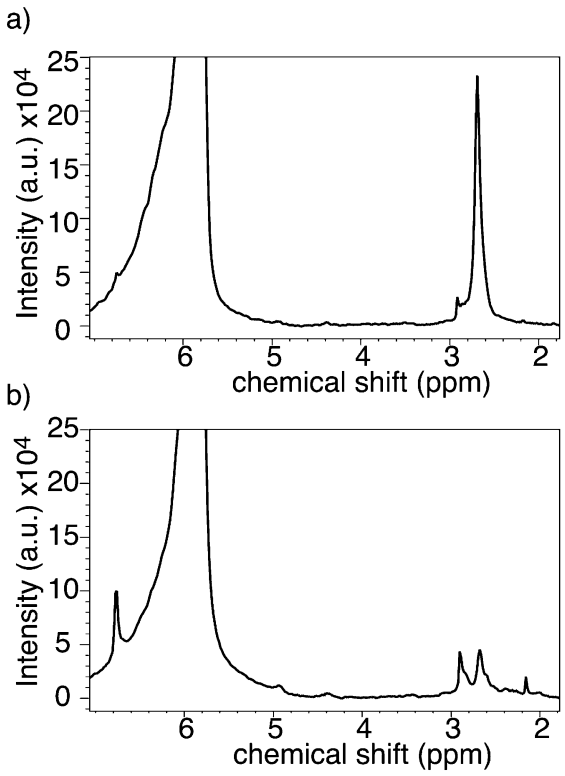

Figure 8. Spectra using the WATERGATE sequence. Spectrum (a) was obtained 600 s after the reagents were mixed and spectrum (b) at 4170 s. Spectra were acquired with eight signal averages, a repetition time of 1 s, and a τ of 660 μs. Peaks at 2.7, 2.93, 5.94, and 6.83 ppm have been identified as CHD, BrCHD, H_2O/H_2SO_4, and Q, respectively. Minor peaks at 4.98 ppm, 4.43, 2.62, 2.17, and 2.0 ppm are also observed; further work is required to assign these.

rotating in a plane normal to the image. To understand these convective patterns, more detailed experiments[34] are required, which follow the flow patterns over a period of time and, with the ability to obtain multislice images rapidly, probe the three-dimensional flow field. This work is currently in progress.

Finally the chemistry of the system was studied using NMR spectroscopy. Spectra for the CHD reaction are show in Figure 7 both preoscillations (a), 10 min after mixing, and during oscillations (b), 70 min after mixing. These spectra were obtained using the P1$\bar{3}3\bar{1}$ sequence and show the chemical shift range 1.8−7.0 ppm. The peaks at 2.7 and 2.9 ppm have been assigned to CHD and BrCHD, respectively. It can be seen that excellent water suppression has been achieved, which is on the order of a factor of 10^3. There is a small peak at 6.83 ppm, which has been assigned to quinone; however its amplitude is reduced as it has been suppressed due to its proximity to the water signal at 5.94 ppm. This quinone peak can be seen better in the WATERGATE spectrum in Figure 8. Here the reduction in amplitude of this peak, associated with suppression of the water signal, is significantly less than that in the P1$\bar{3}3\bar{1}$ experiment. From the excitation profile for the WATERGATE experiment, using a τ of 660 μs, this peak, which is 270 Hz away from the water peak, is reduced by a factor of 0.83 from its original amplitude.

Spectra in Figure 8 also clearly show peaks for CHD and BrCHD. In addition to these peaks another peak at 2.2 ppm can be clearly seen and is also observable in the P1$\bar{3}3\bar{1}$ spectra, Figure 7. The identity of this species is as yet unknown. It is possible that it is another of the organic species found in the reaction mechanism of Szalai et al., such as the enol form of

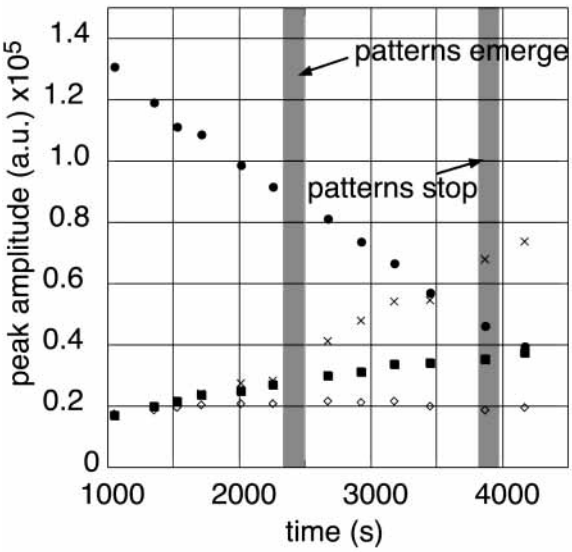

Figure 9. Plot of peak amplitude vs time for CHD (●), BrCHD (■), Q (×), and an unidentified molecule at 1.44 ppm (◇). The peak amplitudes were measured from a series of WATERGATE spectra collected during the CHD reaction. Each spectrum had eight signal averages, a repetition time of 1 s, and a τ of 660 μs.

CHD, CHDE, or 2-cyclohexene-1,4-dione (CHED). However CHED does not have protons that resonate[35] near this chemical shift. The alcoholic proton on CHDE, the enol form of CHD, has a predicted[36] chemical shift closer, at 1.3 ppm, but may not be observable using NMR. However simulations suggest that the concentration of this species is negligible ($\leq 10^{-6}$ mol/L).

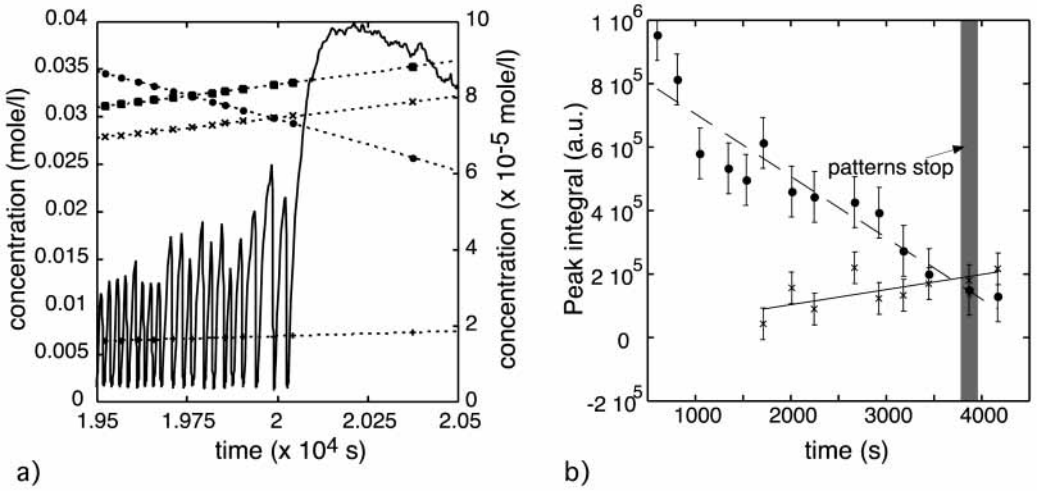

Figure 10. (a) Plot of concentration vs time from the simulated data. The scale on the left-hand side corresponds to the concentration of CHD (●), BrCHD (■), Q (×), and CHDE (+). The scale on the right-hand side corresponds to the concentration of H2Q (−). The initial reaction conditions used in the simulation were [CHD] = 0.1 mol/L, [BrO_3^-] = 0.1 mol/L, and [H^+] = 3.31 mol/L, at a temperature of 293 K. (b) Plot of relative concentration vs time, for CHD (●) and Q (×) from experimental data. Lines of best fit are provided to guide the eye.

Further investigation is required to identify this species. A diffusion coefficient of 1.11×10^{-9} m^2 s^{-1} has been measured for this molecule. Further experiments, including two-dimensional correlation and carbon-13 NMR spectroscopy experiments, are needed to identify this molecule.

The rate of change of CHD, BrCHD, and quinone was followed through measurement of peak amplitudes over time and is shown in Figure 9. The reaction was left unstirred inside the spectrometer, and images of the patterns were also taken. The points at which patterns emerged and finished were detected and have been marked on the plots. The intermediate, hydroquinone, was however not observed. This is most likely due to it being present in very dilute concentration, $\leq 10^{-5}$ mol dm^{-3}, according to simulations of the reaction mechanism.[14] Also its two peaks may be concealed, with the ring protons resonating close to the solvent peak (6.6 ppm) and the alcohol protons exchanging with protons from the solvent. Work is underway to verify the presence of hydroquinone.

Simulations using the reaction mechanism of Szalai and Körös[14] showed that oscillations in the concentration of hydroquinone (H_2Q) ceased just after a point, when the relative concentrations of CHD and quinone became equal. A plot of the simulated concentrations for CHD, BrCHD, quinone, and hydroquinone against time, toward the end of oscillations, is shown in Figure 10a. To verify this observation, from experiment, it is necessary to plot the relative experimental concentrations of CHD and Q molecules and not simply their peak amplitudes. By using the integrals of the peaks and taking into account factors such as the relative number of protons in each molecule, solvent suppression, and relaxation effects, it is possible to have a measure of the relative concentrations of these two species. By plotting these against time, Figure 10b, it can be seen that pattern formation stops at a point just after the concentration of quinone exceeds CHD. By linking the cessation of patterns with the cessation of oscillations, as represented in Figure 9 by the oscillating concentration of hydroquinone, it can be seen that these experiments act, in part, as an independent validation of the proposed mechanism of Szalai and Körös. One difference, of note, between experiment and simulations, which has also been observed by Szalai and co-workers, is the difference in time scale of reaction. In the experimental data the time taken from reaction initiation to the end of oscillations is approximately 4×10^3 s, while in the simulations it is approximately 2×10^4 s. This requires further analysis.

Conclusions

This paper demonstrates the power, and potential, of nuclear magnetic resonance to the study of oscillatory and pattern-forming reactions. Insight into the chemistry and behavior of the 1,4-cyclohexanedione oscillator was achieved through the application of a wide range of NMR techniques. Using MRI experiments, pattern formation was observed in this system. Pulsed gradient spin−echo experiments and flow visualization methods clearly showed the presence of convection for reacting solutions in 10 mm NMR tubes. Spectroscopy experiments have followed the reaction of 1,4-cyclohexanedione and the main reaction intermediates and products. Analysis of the time-dependent concentrations of key organic molecules, CHD and quinone, have in part validated previously proposed reaction mechanisms.

Acknowledgment. M.M.B. thanks EPSRC for an Advanced Research Fellowship, Professor Lynn F. Gladden and the MRRC at Cambridge for support and helpful discussions, and Krisztina Kurin-Csörgei for advice concerning the CHD reaction.

References and Notes

(1) *Oscillations and Traveling Waves in Biological and Chemical Systems*; Field, R. J., Burger, M., Eds.; Wiley: New York, 1985.
(2) Zaikin, A. N.; Zhabotinsky, A. M. *Nature* **1970**, *225*, 535−537.
(3) Armstrong, R. L.; Tzalmona, A.; Menzinger, M.; Cross, A.; Lemaire, C. Imaging the Dynamics of Chemical Waves: the Belousov−Zhabotinsky reaction. In *Magnetic Resonance Microscopy*: *methods and application in materials science, agriculture and biomedicine*; Blümich, B., Kuhn, W., Eds.; VCH: Weinheim, 1992.
(4) Cross, A. R.; Armstrong, R. L.; Reid, A.; Su, S.; Menzinger, M. *J. Phys. Chem.* **1995**, *99*, 16616−16621.
(5) Gao, Y.; Cross, A. R.; Armstrong, R. L. *J. Phys. Chem.* **1996**, *100*, 10159−10164.
(6) Su, S.; Menzinger, M.; Armstrong, R. L.; Cross, A.; Lemaire, C. *J. Phys. Chem.* **1994**, *98*, 2494−2498.
(7) Menzinger, M.; Tzalmona, A.; Armstrong, R. L.; Cross, A.; Lemaire, C. *J. Phys. Chem.* **1992**, *96*, 4725−4727.
(8) Schlüter, A.; Weiss, A. *Ber. Bunsen-Ges. Phys. Chem.* **1981**, *85*, 306−309.
(9) Hansen, E. W.; Ruoff, P. *J. Phys. Chem.* **1989**, *93*, 264−269.
(10) Kurin-Csörgei, K.; Szalai, I.; Körös, E. *React. Kinet. Catal. Lett.* **1995**, *54*, 217−224.
(11) Farage, V. J.; Janjic, D. *Chem. Phys. Lett.* **1982**, *88*, 301−304.
(12) Epstein, I. R.; Pojman, J. A. *An Introduction to Nonlinear Chemical Dynamics*; Oxford University Press: Oxford, 1998.

(13) Kurin-Csörgei, K.; Zhabotinsky, A. M.; Orbán, M.; Epstein, I. R. *J. Phys. Chem.* **1996**, *100*, 5393−5397.
(14) Szalai, I.; Körös, E. *J. Phys. Chem., A* **1998**, *102*, 6892−6897.
(15) Szalai, I.; Kurin-Csorgei, K.; Orban, M. *Phys. Chem. Chem. Phys.* **2002**, *4*, 1271−1275.
(16) Kurin-Csörgei, K.; Szalai, I.; Molnár-Perl, I.; Körös, E. *React. Kinet. Catal. Lett.* **1994**, *53*, 115−121.
(17) Komlósi, A.; Nagy, I. P.; Bazsa, G.; Pojman, J. A. *J. Phys. Chem. A* **1998**, *102*, 9136−9141.
(18) Cavasino, F. P.; Cervellati, R.; Lombardo, R.; Liveri, M. L. T. *J. Phys. Chem. B* **1999**, *103*, 4285−4291.
(19) Bazsa, G.; Epstein, I. R. *J. Phys. Chem.* **1985**, *89*, 3050−3053.
(20) Pojman, J. A.; Epstein, I. R. *J. Phys. Chem.* **1990**, *94*, 4966−4972.
(21) Sakurai, T.; Yokoyama, E.; Miike, H. *Phys. Rev. E* **1997**, *56*, 2367−2370.
(22) Miike, H.; Müller, S. C.; Hess, B. *Phys. Rev. Lett.* **1988**, *61*, 2109−2112.
(23) Callaghan, P. T. *Principles of Nuclear Magnetic Resonance Microscopy*; Oxford University Press: Oxford, 1991.
(24) Eccles, C. http://www.vuw.ac.nz/scps/nmr/Software.html.
(25) Fukushima, E.; Roeder, S. B. W. *Experimental Pulse NMR*: *a Nuts and Bolts Approach*; Addison-Wesley: Reading, MA, 1981.
(26) Hennig, J.; Naureth, A.; Friedburg, H. *Magn. Reson. Med.* **1986**, *3*, 823−833.
(27) Stejskal, E. O.; Tanner, J. E. *J. Chem. Phys.* **1965**, *42*, 288−292.
(28) Morris, G. A.; Freeman, R. *J. Magn. Reson.* **1978**, *29*, 433−462.
(29) Piotto, M.; Saudek, V.; Sklenar, V. *J. Biomol. NMR* **1992**, *2*, 661−665.
(30) Hore, P. J. *J. Magn. Reson.* **1983**, *55*, 283−300.
(31) Derome, A. E. *Modern NMR Techniques for Chemistry Research*; Pergamon Press plc: Oxford, 1987; Vol. 6.
(32) Hinsberg, W. D.; Houle, F. A. Chemical Kinetics Simulator Program; 1.01 ed.; IBM Corporation, available at http://www.almaden.ibm.com/st/msim, 1995.
(33) Hamik, C. T.; Manz, N.; Steinbock, O. *J. Phys. Chem. A* **2001**, *105*, 6144−6153.
(34) Jerschow, A. *J. Magn. Reson.* **2000**, *145*, 125−131.
(35) CHED predicted spectrum, at 400 MHz, with proton resonances at 2 and 3 = 2.44 ppm, 5″ and 6″ = 2.58 ppm, and 5′ and 6′ = 6.47 ppm at http://www.chemweb.com/tools/acdlabs-pred/spec, 2002.

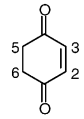

(36) CHDE predicted spectrum, at 400 MHz, with proton resonances at 1′ = 2.62 ppm, 1″ = 2.59 ppm, 2′ = 2.55 ppm, 2″ = 2.62 ppm, 4′ = 2.91 ppm, 4″ = 3.03 ppm, 5 = 5.05 ppm, 7 = 1.44 ppm at http://www.chemweb.com/tools/acdlabs-pred/spec, 2002.